Modified xanthan gum for crystal violet uptake: kinetic, isotherm, and thermodynamic behaviors

Meixia Zheng, Fengli Lian, Yujing Zhu, Bo Liu, Zheng Chen, Yi Zhang, Baodong Zheng and Longtao Zhang

ABSTRACT

Modified xanthan gum (XG-AM-TTE) was employed as an adsorbent to study the adsorption behavior, thermodynamics and kinetics of crystal violet (CV) from an aqueous solution. Fourier transform infrared spectroscopy analysis indicates that the functional groups present in the adsorbent, such as carboxyl, ester and hydroxyl groups, are included on the external surface of the material, and these groups are potential active sites for interaction with CV. According to X-ray diffraction results, the structure of XG-AM-TTE after CV adsorption became more disordered, and the microstructure change is an indication of effective adsorption of CV to the surface, with CV becoming remarkably dispersed in the adsorbent according to the scanning electron microscopy observations. The adsorption kinetics and adsorption equilibrium were best described by the pseudo-second-order model and Freundlich isotherms, respectively. The thermodynamic parameters, as the Gibbs-free energy (ΔG), enthalpy (ΔH) and entropy (ΔS), indicated that the adsorption is a spontaneous, endothermic and entropy increase process. The maximum adsorption capacity of XG-AM-TTE was 183 ± 12 mg/g, suggesting that XG-AM-TTE is an efficient adsorbent.

Key words | adsorption, crystal violet, hydrogel, trimethylolpropane triglycidyl ether, xanthan gum

Meixia Zheng
Yujing Zhu
Bo Liu
Zheng Chen
Agricultural Bio-Resources Research Institute,
Fujian Academy of Agricultural Sciences,
Fuzhou, Fujian 350003,
China

Fengli Lian
Yi Zhang
Baodong Zheng
Longtao Zhang (corresponding author)
College of Food Science,
Fujian Agriculture and Forestry University,
Fuzhou, Fujian 350002,
China;
China-Ireland International Cooperation Centre for
Food Material Science and Structural Design,
Fujian Agriculture and Forestry University,
Fuzhou, Fujian 350002,
China;
and
Fujian Provincial Key Laboratory of Quality Science
and Processing Technology in Special Starch,
Fujian Agriculture and Forestry University,
Fuzhou, Fujian 350002,
China
E-mail: *zlongtao@fafu.edu.cn*

INTRODUCTION

Crystal violet (CV) is always used as a mutagenic and bacteriostatic agent in medical solutions and as an antimicrobial agent to prevent fungal growth in poultry feed. Despite its many uses, CV has been reported as a recalcitrant dye molecule that persists in the environment for a long period of time and poses the threat of toxic effects (Mani & Bharagava 2016). Many works have been conducted on the removal of CV, including adsorption (Hayasi & Karimi 2017), catalytic ozonation (Wang *et al.* 2016), and biodegradation (Kwasniewska 1985). Among these, adsorption has been extensively regarded as an efficient and economically sustainable technology for the removal of CV effluents. Adsorption has received global attention due to its simplicity and flexibility of design, high selectivity and efficiency, low operating cost and high-quality-treated effluents. Thus far, the published research has focused on inorganic adsorbents, such as amino silica (Zhou 2014), magnetic nanocomposite (Singh *et al.* 2011) and Nb_2O_5/SiO_2 (Umpierres *et al.* 2017).

Xanthan gum (XG) is a water-soluble hetero-polysaccharide with many hydrophilic groups in the main chains (Gils Ray & Sahoo 2009), always used as dispersing agent and stabilizer of emulsions and suspensions (Garcíaochoa *et al.* 2000). Its property can be customized and extended by hybridization with synthetic polymers such as acrylamide (AM) (Cheng *et al.* 2017), polyacrylamide (PAM) (Ghorai *et al.* 2014), poly(2-acrylamido-2-methyl-1-propane sulfonic acid)/montmorillonite (P(AMPS)/MMT) (Aflaki *et al.* 2016), polyacrylic acid (PAA) (Li *et al.* 2013), and ethylene diamine tetraacetic acid (EDTA) (Qiu *et al.* 2016). Among these, AM is one of the most important grafting materials. Maia *et al.* (2012) studied the reaction conditions of grafting of AM on XG. Cheng *et al.* (2017) synthesized XG-graft-AM and used as a Cu (II) ion adsorbent. Trimethylolpropane

doi: 10.2166/wst.2019.038

triglycidyl ether (TTE) is a cross-linking agent. Sodium polyacrylate has been grafted on guar gum and the polymers were then surface-crosslinked using TTE to improve its swollen property (Xiong *et al.* 2015). A novel hydrogel base on AM and TTE grafted XG (XG-AM-TTE) demonstrated a conspicuous adsorbing effect for CV in our previous investigation (Zheng *et al.* 2019). Deeply understanding its absorption activity is of practical importance since it affects subsequent processing operations and the application in pollution control.

The kinetic, isotherm, and thermodynamic behaviors of absorption behavior of some absorbents have been reported, such as bottom ash (Mittal *et al.* 2010), XG-g-AM (Cheng *et al.* 2017) and XG-g-P (AMPS)/MMT (Aflaki *et al.* 2016). Several models have been developed to represent the characteristics of absorption behaviors (Cheng *et al.* 2009; Li *et al.* 2013). The pseudo-second-order model was concluded to best predict the kinetics of removal of methylene blue and methyl violet dyes from aqueous solution using a nanocomposite of hydrolyzed polyacrylamide grafted XG and incorporated nanosilica (Ghorai *et al.* 2014). The Gibbs-free energy (ΔG), enthalpy (ΔH) and entropy (ΔS) were used to discuss the thermodynamic behavior of removal of Cu (II) from wastewater by modified XG with ethylene diamine (EDA) (Qiu *et al.* 2016). Different absorbents for different absorbates show various absorption behaviors. The isotherm behavior of XG-PAA for methylene blue is Langmuir (Li *et al.* 2013), the isotherm behavior of XG-g-AM for Cr (III) is Freundlich (Cheng *et al.* 2009), and the isotherm behavior of XG-g-AM for Cu (II) is Langmiur and Freundlich (Cheng *et al.* 2017). So far, the kinetic, isotherm, and thermodynamic behaviors of XG-AM-TTE for CV have not been reported.

The main objective of this study was to evaluate the absorption behavior of removing CV using XG-AM-TTE. Adsorbent experiments were carried out to investigate the effects of the adsorbent XG-AM-TTE dose, initial pH, contact time, temperature and initial CV concentration.

MATERIALS AND METHODS

Materials

Xanthan gum (XG, USP, PubChem CID: 7107) was purchased from Aladdin Industrial Corporation. Its CAS number is 11138-66-2, its molecular formula is $C_{35}H_{49}O_{29}$, and it is moisture sensitive. Acrylamide (AM, AR, 99.0%, PubChem CID: 6579; C_3H_5NO) was purchased with a molar mass of 71.08 g/mol. Trimethylolpropane triglycidyl ether (TTE, Tech, PubChem CID: 103015) was purchased from Sigma-Aldrich. All other chemical reagents were of analytical grade.

Synthesis of modified xanthan gum hydrogel

The modified XG (XG-AM-TTE) was synthesized in a four-necked flask under a pure nitrogen gas environment and equipped with a mechanical stirrer, a thermometer, and a reflux condenser. An aliquot of 1 g XG was dissolved in 150 mL distilled water under constant stirring for 60 min at room temperature. Then, AM (15 g) and 260 μL TTE were added sequentially into the XG solution, and the resulting mixture was stirred and saturated with pure nitrogen to remove the dissolved oxygen. The temperature was held at 70 °C, and 0.3 g of potassium persulfate (KPS) was added and reacted for 4 h to initiate the graft copolymer. The precipitate was filtered, washed thoroughly with an ethanol/water mixture (v: v = 4:1) three times under high-speed stirring, and soaked in the ethanol/water mixture (v: v = 4:1) for 24 h. The XG-AM-TTE was collected by filtration and freeze drying.

Characterization of XG-AM-TTE

Fourier transform infrared spectroscopy (FT-IR) analysis

FT-IR spectra of XG-AM-TTE before and after CV absorption were recorded in the solid state using KBr pellets with an AVATAR 360 FT-IR spectrometer in the range from 400 to 4,000 cm^{-1} at 2 cm^{-1} resolution.

X-ray diffraction (XRD) analysis

The structures of XG-AM-TTE before and after CV absorption were investigated using an Empyrean XRD instrument (Rigaku, Miniflex 600) with a Cu Kα1 radiation source. The X-ray generator was operated at 40 kV and 15 mA. The reflection angle 2θ was monitored from 5° to 60° at a scanning speed of 10°/min and a step size of 0.02 (λ = 1.5406 nm).

Microstructure analysis

The microstructures of XG-AM-TTE before and after CV absorption were examined by a scanning electron microscope (SEM) (JSM-6380LV, JEOL), operating with

secondary electrons under low vacuum at 15.0 kV. The samples were coated with Au prior to the SEM examination.

Batch adsorption experiments

A certain amount of XG-AM-TTE and 100 mL of CV solution was sealed in a 250 mL conical flask with a cap to minimize evaporation. Adsorption was allowed to proceed at 25 °C at 170 rpm in a thermostatic shaker for a predetermined time. The pH of the solution was adjusted to the desired values using 0.1 M HCl or 0.1 M NaOH with stirring before the addition of XG-AM-TTE and then shaken in a constant-temperature water bath. CV concentrations in the bulk solutions were analyzed using an xMark (BioRad) instrument at 590 nm.

The adsorption capacity (Q_e, mg/g) and the removal rate (η, %) were calculated using Equations (1) and (2), respectively.

$$Q_e = (C_iV_i - C_eV_e)/m \quad (1)$$

$$\eta = (C_iV_i - C_eV_e)/C_iV_i \times 100\% \quad (2)$$

where C_i and C_e are the initial and final CV concentrations (mg/L), respectively, V_i and V_e are the initial and final volume of CV (L), and m is the weight in grams of XG-AM-TTE used for the adsorption measurements (g).

RESULTS AND DISCUSSION

Characteristics of XG-AM-TTE

The FT-IR spectra of XG-AM-TTE before and after CV adsorption are shown in Figure 1. XG-AM-TTE shows a broad peak at 3,449 cm^{-1} due to the stretching vibrations of O-H and N-H. The peaks at 1,655 cm^{-1} and 1,611 cm^{-1} are attributed to amide-I (the C = O stretching vibrations) and amide-II (the N-H bending vibrations). The peak at 1,655 cm^{-1} is due to the characteristic absorption of $CONH_2$, the peak at 1,420 cm^{-1} is due to stretching vibrations of C-N, and the peak at 1,117 cm^{-1} is due to the wagging vibration of NH_2. Examination of the FT-IR spectrum obtained after CV adsorption shows that the frequencies and intensities of some peaks have shifted or substantially decreased compared to their preadsorption values. This can be ascribed to the occurrence of a complex process between the ionizable functional groups and CV. The chemical structure of CV is shown in Figure S1

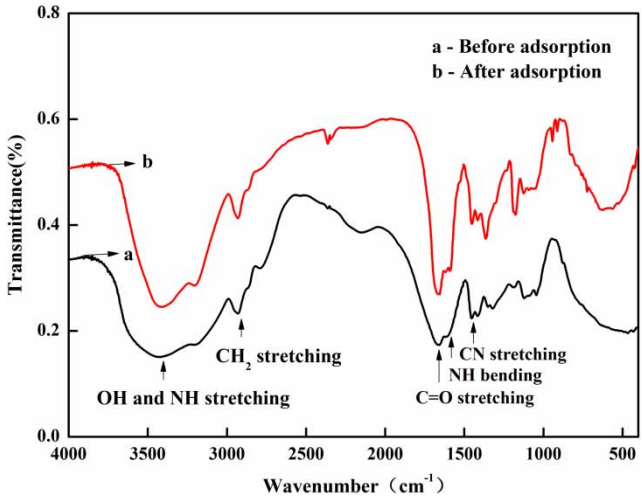

Figure 1 | FT-IR spectra from 4,000 to 400 cm^{-1} of XG-AM-TTE before (black line, a) and after (red line, b) CV adsorption. The full color version of this figure is available in the online version of this paper, at http://dx.doi.org/10.2166/wst.2019.038.

(available with the online version of this paper). The FT-IR analysis results indicate that the functional groups present in the adsorbent, such as the carboxyl, ester and hydroxyl groups, are included in the external surface of the material, and these groups can be the potential active sites for interaction with CV.

The XRD measurements probed the crystal behavior of the sample. The XRD patterns of XG-AM-TTE before and after CV absorption are displayed in Figure 2. As seen, there is no specific peak in the XRD spectrum of XG-AM-TTE before and after CV adsorption, implying that the

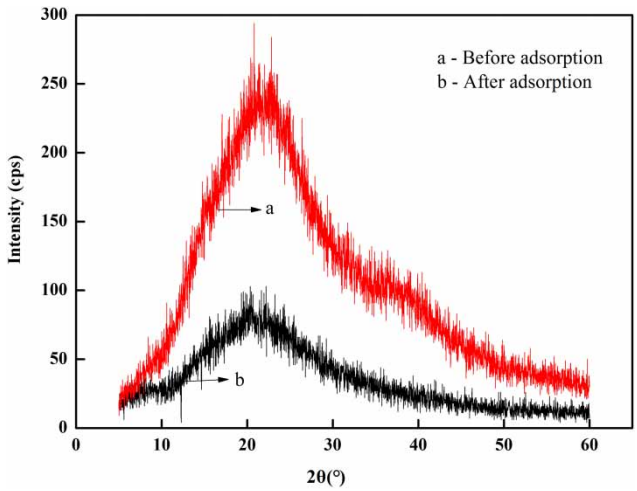

Figure 2 | X-ray diffraction pattern of XG-AM-TTE before (red line, a) and after (black line, b) CV adsorption. The X-ray generator was operated at 40 kV and 15 mA. The XRD chromatograms were recorded over an angular range of 5° to 60° (2θ) at a scanning speed of 10°/min and a step size of 0.02 (λ = 1.5406 nm). The full color version of this figure is available in the online version of this paper, at http://dx.doi.org/10.2166/wst.2019.038.

XG-AM-TTE before and after CV adsorption is almost amorphous and revealing that there are covalent bonds inside the XG-AM-TTE. The peak becomes broad after the introduction of CV, so it is possible that the CV destroyed the covalent bonding in the material, making its structure more disordered.

The SEM images of the surface structure of the XG-AM-TTE before and after CV adsorption are shown in Figure 3. It is clear that, prior to adsorption, the external surface of the sample is rough and irregular and contains pores of different sizes and shapes, causing the CV to become trapped and adsorbed into these different parts of the adsorbent. After adsorption, welling and drying are carried out; a significant change is observed in the structure of the XG-AM-TTE, which can be taken as an indication of effective adsorption of CV to the surface and makes the CV become remarkably dispersed in the adsorbent.

Effect of adsorbent dose

The adsorbent dose is one of the parameters that strongly affect the adsorption capacity in an aqueous solution (Zafar *et al.* 2008). The efficiency of mass dosage of the adsorbent was studied by agitating the different masses (0.05, 0.15, 0.25, 0.35, 0.5, 0.75, 1 and 2 g/L) of XG-AM-TTE and 100 mL of 30 mg/L CV using a shaker at room temperature. The experiments were conducted at an optimized pH of 7.0. The results of the experiments with varying adsorbent doses are presented in Figure 4. Increasing the XG-AM-TTE dose resulted in an increase in the CV removal. More specifically, the increase rate of this parameter was high for higher XG-AM-TTE doses due to the greater availability of active sites on the surface of the materials and low for lower XG-AM-TTE doses due to the progressive saturation of these active sites (Saha *et al.* 2010). However, the amount of CV adsorbed per XG-AM-TTE mass unit decreased considerably as the XG-AM-TTE dose increased. This can be attributed to the adsorption sites remaining unsaturated during the adsorption reaction (Chowdhury & Saha 2010). These results were in agreement with other similar studies on CV adsorption (Saeed *et al.* 2010). In addition, it could also be noticed that for the majority of the tested materials, the steady state was reached for an adsorbent dose between 0.25 and 0.75 g/L. Therefore, the optimum adsorbent dose of 0.75 g/L was selected for use in all subsequent experiments.

Effect of initial pH on adsorption of CV

The pH of an aqueous solution plays an important role in controlling the parameters in the dye adsorption process because it affects the surface charge of the sorbent material and the degree of ionization of the dye molecule (Ramakrishnan & Nagarajan 2009). pH has been related to changes in the structural stability and color intensity of the dye molecule and charged chromophore (Monash & Pugazhenthi 2009). Figure 5 shows the effects of an initial pH in the 2.0–6.0 range on the equilibrium adsorption capacity of CV on XG-AM-TTE. The results show that the Q_e of CV on the XG-AM-TTE, as well as η, increases as the initial solution pH increases in the 2.0–7.0 range. The maximum Q_e and η of CV were obtained at pH 7.0. This can be explained as being due to the availability of dye-binding sites on the XG-AM-TTE at these pH values. The poor Q_e and η of the

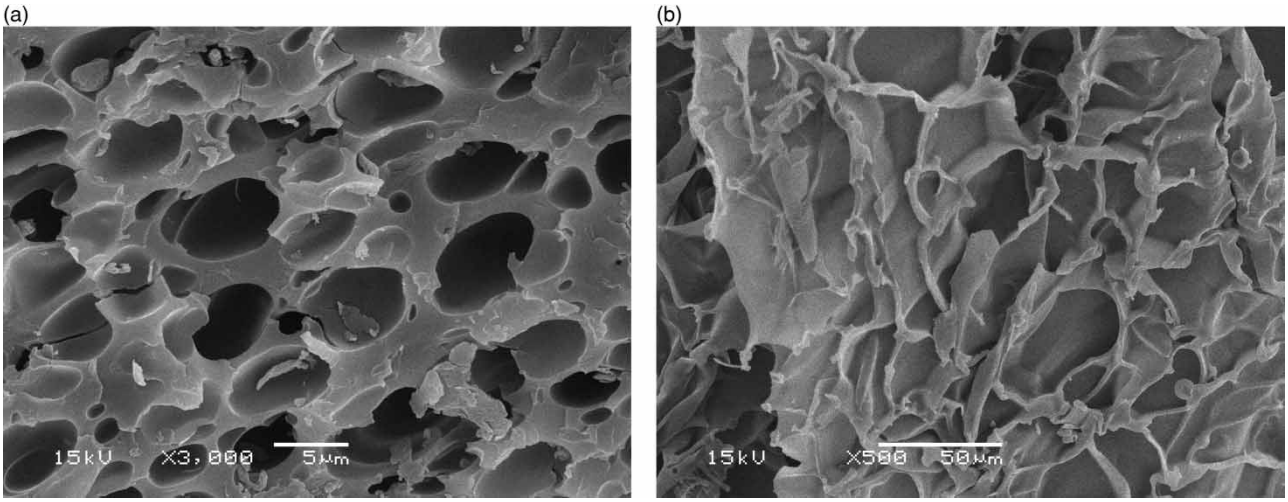

Figure 3 | SEM micrograph of XG-AM-TTE before ((a) ×3000) and after ((b) ×500) CV adsorption. SEM analyses were performed using a JSM-6380LV (JEOL) operated with an accelerating voltage of 15.0 kV. The samples were coated with Au prior to the experiment.

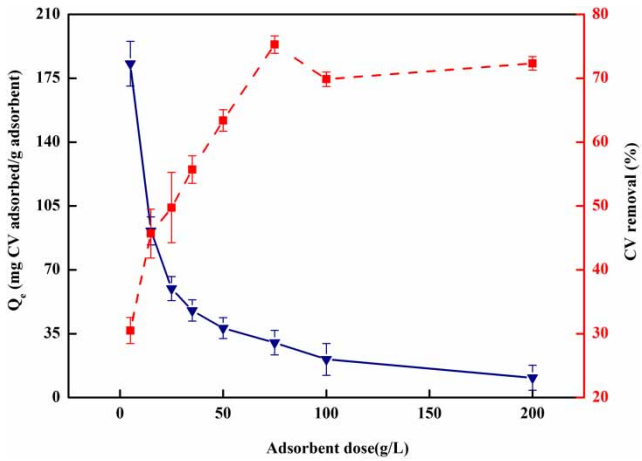

Figure 4 | Effect of mass dosage of adsorbent on the adsorption capacity (continuous line) and the removal (dotted line) of CV by XG-AM-TTE at room temperature, with a contact time of 60 min, a 30 mg/L dye concentration and pH 7.0. The error bars represent the standard error.

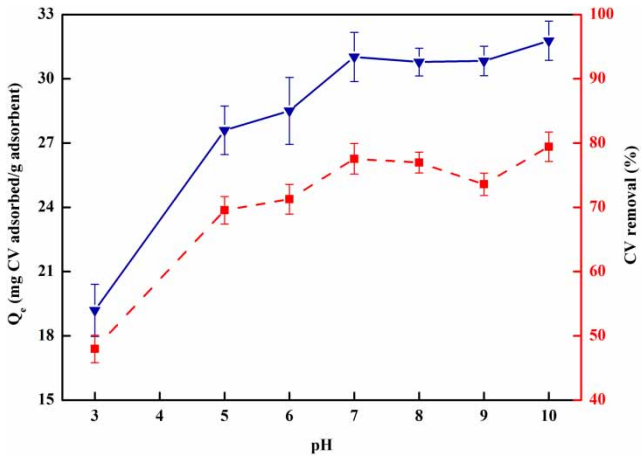

Figure 5 | Effect of pH on the adsorption capacity (continuous line) and the removal (dotted line) of CV by XG-AM-TTE at room temperature, with a contact time of 60 min, and a 30 mg/L dye concentration. The error bars represent the standard error.

XG-AM-TTE in the low-pH region is attributed to the large number of hydrogen ions in acidic conditions, which gives rise to high mobility and competition with CV for the active sites on the XG-AM-TTE, leading to reduced attraction between the XG-AM-TTE and greater Q_e and η. The Q_e and η values tend to be stable with an increase in pH in the range of 7.0–10.0. Therefore, all subsequent studies were carried out at pH 7.0 as the optimum pH.

Effect of contact time

Contact time is an important parameter for the assessment of the prospects for the practical application of the adsorption process (Jethave *et al.* 2017). Figure 6 shows the Q_e and η of CV in the contact time range of 0–90 min with an initial CV concentration of 30 mg/L and an XG-AM-TTE concentration of 0.75 g/L at pH 7.0. By increasing the contact time, increases in both the amount of CV adsorbed per XG-AM-TTE mass unit and the CV removal were obtained. The η of CV was increased by the contact time so that approximately 58% of CV removal occurred in the first 10 min. In most cases, the rapid initial adsorption during the first few minutes of contact was followed by a slower adsorption process until an equilibrium state was reached. This was due to the existence of abundant vacant active sites, on which adsorption continued with progressive saturation of these active sites with longer times. In addition, the required time to reach equilibrium was approximately 30–90 min because an increase in the contact time to 90 min did not have any significant effects. A short equilibrium time indicates that CV has a high tendency for rapid migration and diffusion to the XG-AM-TTE surface. Therefore, the rest of the experiments were performed using a 30 min contact time.

Effect of initial CV concentration

The mechanism of CV adsorption from an aqueous solution is particularly dependent on the initial CV concentration in the solution. Figure 7 shows the Q_e and η of CV in the initial CV concentration range of 10–50 mg/L, with 0.75 g/L XG-AM-TTE at pH 7.0. Increasing the initial CV concentration caused an increase in the amount of CV adsorbed per XG-

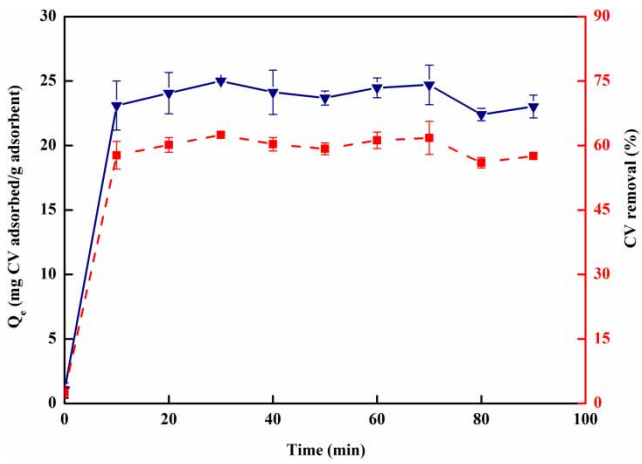

Figure 6 | Effect of contact time on the adsorption capacity (continuous line) and the removal (dotted line) of CV by XG-AM-TTE at room temperature and pH 7.0, with an adsorbent dosage of 75 mg in 100 mL and a 30 mg/L dye concentration. The error bars represent the standard error.

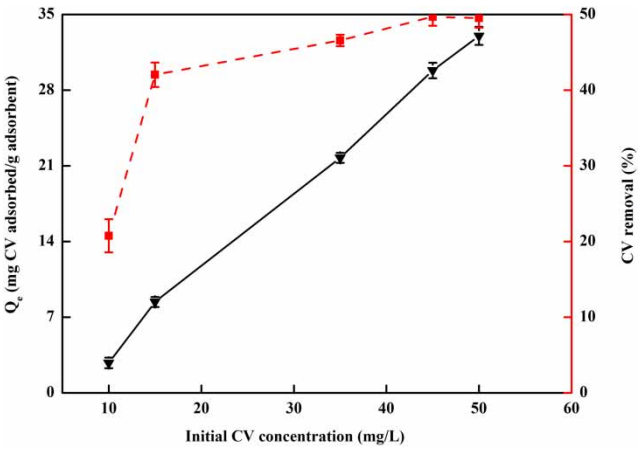

Figure 7 | Effect of the initial CV concentration (10, 15, 35, 45, 50 mg/L) on the adsorption capacity (continuous line) and the removal (dotted line) of CV by XG-AM-TTE at room temperature and pH 7.0, with an adsorbent dosage of 75 mg in 100 mL. The error bars represent the standard error.

AM-TTE mass unit. This was due to the increase in the concentration gradient, which is the driving force for mass transfer.

Effect of contact temperature

Figure 8 presents the effect of contact temperature on CV adsorption and removal. The adsorption and removal of CV were achieved at 0.75 g/L XG-AM-TTE, an initial CV concentration of 30 mg/L and pH 7.0. By increasing the contact temperature, an increase in both the amount of CV adsorbed per XG-AM-TTE mass unit and the CV removal was obtained. This may be attributed to the lower solvent viscosity and higher average kinetic energy of ions

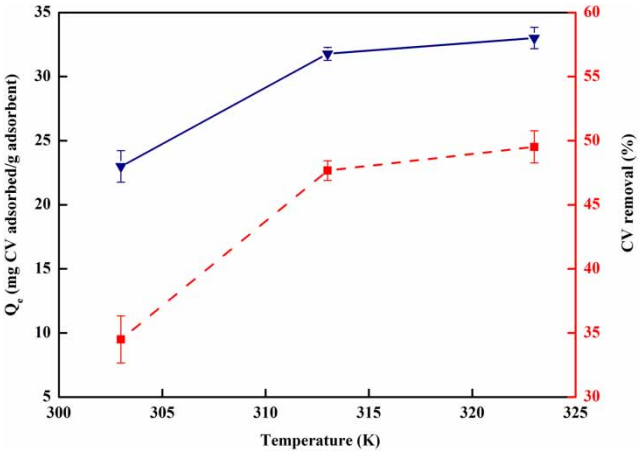

Figure 8 | Effect of contact temperature on the amount of CV adsorbed per adsorbent mass unit (continuous line) and on the CV removal percentage (dotted line). The error bars represent the standard error.

under high-temperature conditions. This fact suggests that the adsorption of CV is endothermic in nature. Therefore, to reduce the operational costs, the experiments were performed at 303 K.

Adsorption kinetics

To study the kinetics of CV adsorption, three kinetic models were applied (Pellera *et al.* 2012): the pseudo-first-order model (Equation (3)), the pseudo-second-order model (Equation (4)) and the intraparticle diffusion model (Equation (5)).

$$\log(Q_e - Q_t) = \log(Q_e) - k_1 t/2.303 \quad (3)$$

$$t/Q_t = 1/k_2 Q_e^2 + t/Q_e \quad (4)$$

$$Q_t = k_{id} t^{1/2} + C \quad (5)$$

where k_1 is the adsorption rate constant (min^{-1}), t is the time (min), Q_e and Q_t are the amounts of CV adsorbed per adsorbent mass unit at equilibrium and at time t (mg/g), respectively, and $Q_{e;exp}$ and $Q_{e;calc}$ are the amounts of CV adsorbed per adsorbent mass unit at equilibrium (mg/g), obtained from the experiments with varying contact time (experimental) and from the fitting to the pseudo-first-order model (calculated), respectively. k_2 is the adsorption rate constant (g/mol/min), and $h = k_2 Q_e^2$ represents the initial adsorption rate for the pseudo-second-order model. Finally, k_{id} is the adsorption rate constant ($mol/g/min^{1/2}$), and C is the intraparticle diffusion constant.

The results shown in Table 1 indicate that the pseudo-second-order model provides the best description of the CV adsorption kinetics for XG-AM-TTE. This is demonstrated by its correlation coefficient value of 0.9981, as well as by the Q_e value of 25.84 mg/g, which was very close to the experimental value of $Q_{e;exp}$ of 25.77 mg/g. This implies that the adsorption process is probably a chemical process (Wu *et al.* 2009), and it could be rate limiting in the sorption step involving the ion exchange of the sorbent and sorbate. In the intraparticle diffusion model, the linear plots passing through the origin indicate that single particle diffusion is the rate-limiting step (Lorenc-Grabowska & Gryglewicz 2005). However, in this study, the linear plots do not pass through the origin, which may be due to the difference in the rate of mass transfer in the process of adsorption and also shows that the intraparticle diffusion model is not the only rate-limiting step. Particle diffusion and boundary layer diffusion interactions affect the adsorption of CV on XG-AM-TTE as well. In the description of the

Table 1 | Kinetics parameters for CV adsorption onto XG-AM-TTE

	Pseudo-first-order model			Pseudo-second-order model				Intraparticle diffusion model		
$Q_{e,\ exp}$ mg/g	k_1 min^{-1}	$Q_{e,calc}$ mg/g	R^2	k_2 g/mg/min	Q_e mg/g	$h = k_2 Q_e^2$	R^2	k_3 mg/g/$min^{1/2}$	C	R^2
25.77	0.084	14.39	0.9368	0.034	25.84	22.94	0.9981	0.839	19.64	0.9208

adsorption kinetics by the pseudo-second-order and the intraparticle diffusion models, the rate-limiting step is chemical sorption (chemisorption) between the XG-AM-TTE and the CV. For the pseudo-first-order model and the intraparticle diffusion model, although in some cases the correlation coefficient values were quite high ($R^2 > 0.9$), the value of $Q_{e;calc}$ (14.39 mg/g) was much lower than the experimental value of $Q_{e;exp}$ (25.77 mg/g). The applicability of the pseudo-second-order model to the materials examined in this study is in agreement with the result obtained by Mittal (Mittal *et al.* 2010).

Equilibrium isotherms

The equilibrium adsorption isotherm provides some of the most important data for the description of the adsorption behavior of an adsorption system. The adsorption process is normally described by the Henry (Equation (6)), Langmuir (Equation (7)) and Freundlich isotherms (Equation (8)) (Chen *et al.* 2016).

$$Q_e = K_d C_e \tag{6}$$

$$C_e/Q_e = 1/bQ + C_e/Q \tag{7}$$

$$\lg Q_e = \lg K_f + 1/n \lg C_e \tag{8}$$

where K_d is the linear adsorption coefficient (L/g), Q_e is the amount of CV adsorbed per XG-AM-TTE mass unit (mg/g) at equilibrium, C_e is the equilibrium CV concentration in the solution (mg/L), Q is the maximum dye uptake (mg/g), b is the adsorption energy (L/mg), K_f is the distribution coefficient (mg/g(L/mg)$^{1/n}$) indicating the adsorption capacity (L/g), n is the heterogeneity factor, indicating the degree of nonlinearity, and 1/n is a dimensionless parameter indicating adsorption intensity.

The results obtained from the application of the three isotherms are shown in Table 2. It can be seen that the Freundlich isotherm provided the best description of the adsorption equilibrium, with high correlation coefficient values ($R^2 > 0.99$). This suggests monolayer coverage of the surface of XG-AM-TTE by CV, indicative that the adsorption was surface adsorption. This also shows the inhomogeneity on the surface of XG-AM-TTE, the reversibility of the adsorption and the coexistence of various interactions, as suggested by FT-IR, XRD and SEM.

Thermodynamic parameters

The mechanism of adsorption may be determined through thermodynamic quantities such as the change in ΔS, ΔG, and ΔH. The thermodynamic equilibrium constant K can be calculated using Equation (9) and the increase in K with an increase in temperature indicates the endothermic nature of the process. The ΔS, ΔG and ΔH values were calculated using the van 't Hoff equation, given by Equations (10) and (11) (Chen *et al.* 2016).

$$K_d = Q_e/C_e \tag{9}$$

$$\ln K_d = -\Delta H/RT + \Delta S/R \tag{10}$$

$$\Delta G = \Delta H - T\Delta S \tag{11}$$

where K_d is the thermodynamic equilibrium constant (L/mol), Q_e is the amount of CV adsorbed per adsorbent mass unit (mg/g) at equilibrium, C_e is the equilibrium CV concentration in the solution (mg/L), R is the universal gas constant (8.314 J/mol^{-1}/K), T is the temperature (K), ΔS is the entropy (J/mol/K), ΔH is the change in the enthalpy of adsorption (J/mol), and ΔG is the Gibbs-free energy (J/mol).

Table 2 | Adsorption equilibrium parameters

Henry		Langmuir			Freundlich		
K (L/g)	R^2	Q (mg/g)	b (L/mg)	R^2	K (mg/g/(L/mg)$^{1/n}$)	1/n	R^2
1.0022	0.9626	−7.7882	−0.0351	0.8878	0.0296	2.2067	0.9918

Using linear regression analysis, the values of ΔH and ΔS are determined from the intercept and slope of the plot of ΔG vs. T according to Equation (10). The calculated thermodynamic parameters are listed in Table 3. The thermodynamic constants at an initial CV concentration of 50 mg/L were calculated. The positive value of ΔH is indicative of the endothermic nature of the adsorption interaction, which is consistent with the adsorption increasing with increasing temperature. The positive value of ΔS shows the affinity of CV and the increasing randomness at the solid-solution interface during the adsorption process, which is consistent with the XRD results. The decrease in the negative value of ΔG with temperature shows that the adsorption process becomes more favorable at higher temperatures, and the negative value of ΔG over all of the examined temperature range also indicates the feasibility of the adsorption process and the spontaneous nature of CV adsorption. Adsorption of CV appears to be spontaneous and endothermic. ΔG is less than −80 kJ/mol, indicate that, the adsorption was chemical adsorption.

Table 3 | Thermodynamic parameters for the adsorption of CV

ΔH (J/mol)	ΔS (J/mol/K)	ΔG (J/mol)	
		313 K	323 K
24,489.72	79.06	−256.16	−1,046.77

Adsorption capacity

The adsorption capacities and adsorption behavior of various adsorbents included modified XG were compared in Table 4. For the same absorbate, XG-AM-TTE showed higher adsorption capacity on CV than inorganic adsorbent, such as Nb_2O_5/SiO_2 (116 mg/g) (Umpierres *et al.* 2017), magnetic nanocomposite (112 mg/g) (Singh *et al.* 2011), and amino silica (40 mg/g) (Zhou 2014). While, it showed lower adsorption capacity on CV than bottom ash (887 mg/g) (Mittal *et al.* 2010), which was inferred to be activated carbon. The other modified XG has also been reported and been used to adsorb dyes and heavy metals (Table 4). XG-g-AM showed the highest absorption capacity on heavy metals (Cheng *et al.* 2009). XG-PAM showed higher absorption capacity on methyl violet (Ghorai *et al.* 2014). In this work, the modified XG, XG-AM-TTE, showed absorption capacity on CV.

Table 4 | Comparison of the adsorption capacities of various adsorbents

Adsorbents	Absorbate	Q_e (mg/g)	Kinetic	Isotherm	Thermodynamic	Reference
Mino silica	Crystal violet	40	–	–	–	Zhou (2014)
Magnetic nanocomposite	Crystal violet	112	–	–	–	Singh *et al.* (2011)
Nb_2O_5/SiO_2	Crystal violet	116	–	–	–	Umpierres *et al.* (2017)
Bottom ash	Crystal violet	887	Pseudo-second order	Langmuir	Spontaneous endothermic entropy increase	Mittal *et al.* (2010)
XG-g-AM	Cu(II)	–	Pseudo-second order	Langmiur, Freundlich	Spontaneous endothermic entropy increase	Cheng *et al.* (2017)
XG-g-P(AMPS)/MMT	Cu(II)	29	Pseudo-second order	Langmuir	Spontaneous endothermic entropy increase	Aflaki *et al.* (2016)
XG-PAA	Methylene blue	30	–	Langmuir	–	Li *et al.* (2013)
XG-EDA	Cu(II)	46	Pseudo-second order	Langmuir	–	Qiu *et al.* (2016)
XG-g-AM	Cr(III)	205	Pseudo-second order	Freundlich	–	Cheng *et al.* (2009)
XG-PAM	Methyl violet	378	Pseudo-second order	Langmuir	–	Ghorai *et al.* (2014)
XG-AM-TTE	Crystal violet	183 ± 12	Pseudo-second order	Freundlich	Spontaneous endothermic entropy increase	This work

AM is acrylamide, AMPS is 2-acrylamido-2-methyl-1-propane sulfonic acid, MMT and OMMT are montmorillonite, EDA is ethylenediamine, PAM is polyacrylamide, PAA is polyacrylic acid, TTE is trimethylolpropane triglycidyl ether, Q_e is the absorption capacity.

CONCLUSION

The adsorption behavior of XG-AM-TTE for CV was investigated. Various impact factors, such as adsorbent dose, pH, contact time, temperature and initial CV concentration, were optimized. The experimental results can fit perfectly with the pseudo-second-order model and the Freundlich isotherm model. A negative value of ΔG and a positive value of ΔH confirm the spontaneous and endothermic nature of the adsorption process. The adsorption process is mainly controlled by both surface and chemical reactivity and obeys the pseudo-second-order model for the entire adsorption period. Overall, XG-AM-TTE is an effective adsorbent for the removal of CV from aqueous solutions.

ACKNOWLEDGEMENTS

This work was supported by International Science and Technology Cooperation and Exchange Program of Fujian Agriculture and Forestry University (KXGH17001), Fujian Provincial Foreign Cooperation Project (2018I0003), Fujian Provincial Science and Technology Program of Regional Development Project (2018N3001) and National Natural Science Foundation of China (31628016).

REFERENCES

Aflaki, J. M., Dadvand, K. A. & Sheykhan, M. 2016 Experimental study of the removal of copper ions using hydrogels of xanthan, 2-acrylamido-2-methyl-1-propane sulfonic acid, montmorillonite: kinetic and equilibrium study. *Carbohydrate Polymers* **142**, 124–132.

Chen, J. F., Zhang, W. Y. & Li, X. 2016 Adsorption of Cu(II) ion from aqueous solutions on hydrogel prepared from Konjac glucomannan. *Polymer Bulletin* **73**, 1965–1984.

Cheng, L., Li, Z. J., Wang, L., Zhu, X. F. & Zhang, C. W. 2009 Adsorption characteristic of graft copolymers of xanthan gum and acrylamide for Cr^{3+}. *Fine Chemicals* **28** (12), 2185–2188.

Cheng, L., Cheng, L. H. & Wang, X. Y. 2017 Thermodynamics and kinetics for Cu(II) adsorption by graft copolymer of xanthan gum and acrylamide. *Journal of Materials Science & Engineering* **35** (4), 553–558, 581.

Chowdhury, S. & Saha, P. 2010 Sea shell powder as a new adsorbent to remove Basic Green 4 (Malachite Green) from aqueous solutions: equilibrium, kinetic and thermodynamic studies. *Chemical Engineering Journal* **164** (1), 168–177.

Garcíaochoa, F., Santos, V. E., Casas, J. A. & Gomez, E. 2000 Xanthan gum: production, recovery, and properties. *Biotechnology Advances* **18** (7), 549–579.

Ghorai, S., Sarkar, A., Raoufi, M., Panda, A. B., Schonherr, H. & Pal, S. 2014 Enhanced removal of methylene blue and methyl violet dyes from aqueous solution using a nanocomposite of hydrolyzed polyacrylamide grafted xanthan gum and incorporated nanosilica. *ACS Applied Materials & Interfaces* **6** (7), 4766–4777.

Gils, P. S., Ray, D. & Sahoo, P. K. 2009 Characteristics of xanthan gum-based biodegradable superporous hydrogel. *International Journal of Biological Macromolecules* **45** (4), 364–371.

Hayasi, M. & Karimi, M. 2017 Synthesis of poly(styrene-co-methacrylic acid)-coated magnetite nanoparticles as effective adsorbents for the removal of crystal violet and Rhodamine B: a comparative study. *Polymer Bulletin* **74** (6), 1995–2016.

Jethave, G., Fegade, U., Attarde, S. & Ingle, S. 2017 Facile synthesis of lead doped zinc-aluminum oxide nanoparticles (LD-ZAO-NPs) for efficient adsorption of anionic dye: kinetic, isotherm and thermodynamic behaviors. *Journal of Industrial & Engineering Chemistry* **53**, 294–306.

Kwasniewska, K. 1985 Biodegradation of crystal violet (hexamethyl-*p*-rosaniline chloride) by oxidative red yeasts. *Bulletin of Environmental Contamination and Toxicology* **34** (1), 323–330.

Li, S., Liu, G. Q., Liang, D. D., Liu, Y. & Liao, J. E. 2013 Synthesis of polyacrylic acid hydrogel grafted with xanthan gum and its adsorption properties for methylene blue. *Adhesion* **37** (12), 57–60.

Lorenc-Grabowska, E. & Gryglewicz, G. 2005 Adsorption of lignite-derived humic acids on coal-based mesoporous activated carbons. *Journal of Colloid & Interface Science* **284** (2), 416–423.

Maia, A. M., Silva, H. V., Curti, P. S. & Balaban, R. C. 2012 Study of the reaction of grafting acrylamide onto xanthan gum. *Carbohydrate Polymers* **90** (2), 778–783.

Mani, S. & Bharagava, R. N. 2016 Exposure to crystal violet, its toxic, genotoxic and carcinogenic effects on environment and its degradation and detoxification for environmental safety. *Reviews of Environmental Contamination & Toxicology* **237** (12), 71–104.

Mittal, A., Mittal, J., Malviya, A., Kaur, D. & Gupta, V. K. 2010 Adsorption of hazardous dye crystal violet from wastewater by waste materials. *Journal of Colloid & Interface Science* **343** (2), 463–473.

Monash, P. & Pugazhenthi, G. 2009 Adsorption of crystal violet dye from aqueous solution using mesoporous materials synthesized at room temperature. *Adsorption* **15** (4), 390–405.

Pellera, F. M., Giannis, A., Kalderis, D., Anastasiadou, K., Stegmann, R., Wang, J. Y. & Gidarakos, E. 2012 Adsorption of Cu(II) ions from aqueous solutions on biochars prepared from agricultural by-products. *Journal of Environmental Management* **96** (1), 35–42.

Qiu, H., Yan, J., Lan, G., Liu, Y., Song, X., Peng, W. & Cui, Y. 2016 Removal of Cu^{2+} from wastewater by modified xanthan gum (XG) with ethylenediamine (EDA). *RSC Advances* **6** (86), 1–9.

Ramakrishnan, M. & Nagarajan, S. 2009 Utilization of waste biomass for the removal of basic dye from water. *World Applied Sciences Journal* **5**, 114–121.

Saeed, A., Sharif, M. & Iqbal, M. 2010 Application potential of grapefruit peel as dye sorbent: kinetics, equilibrium and mechanism of crystal violet adsorption. *Journal of Hazardous Materials* **179** (1–3), 564–572.

Saha, P., Chowdhury, S., Gupta, S. & Kumar, I. 2010 Insight into adsorption equilibrium, kinetics and thermodynamics of Malachite Green onto clayey soil of Indian origin. *Chemical Engineering Journal* **165** (3), 874–882.

Singh, K. P., Gupta, S., Singh, A. K. & Sinha, S. 2011 Optimizing adsorption of crystal violet dye from water by magnetic nanocomposite using response surface modeling approach. *Journal of Hazardous Materials* **186** (2–3), 1462–1473.

Umpierres, C. S., Prola, L. D., Adebayo, M. A., Lima, E. C., Dos Reis, G. S., Kunzler, D. D., Dotto, G. L., Arenas, L. T. & Benvenutti, E. V. 2017 Mesoporous Nb_2O_5/SiO_2 material obtained by sol-gel method and applied as adsorbent of crystal violet dye. *Environmental Technology* **38** (5), 566–578.

Wang, Z., Wu, J., Li, Z. & Zhan, X. 2016 Characterization of xanthan gum produced from glycerol by a mutant strain *Xanthomonas campestris* CCTCC m2015714. *Carbohydrate Polymers* **157**, 521–526.

Wu, Y., Zhang, L., Gao, C., Ma, J., Ma, X. & Han, R. 2009 Adsorption of copper ions and methylene blue in a single and binary system on wheat straw. *Journal of Chemical & Engineering Data* **54** (54), 3229–3234.

Xiong, Y., Zhang, X. & Liu, M. Z. 2015 Surface-crosslinked guar gum-g-sodium poly-acrylate superabsorbents: swelling characteristics and mechanics performance. *Applied Mechanics and Materials* **729**, 39–46.

Zafar, S. I. B. M., Saeed, A. & Iqbal, M. 2008 FTIR spectrophotometry, kinetics and adsorption isotherms modeling, and SEM-EDX analysis for describing mechanism of biosorption of the cationic basic dye methylene blue by a new biosorbent (sawdust of silver fir; *Abies pindrow*). *Fresenius Environmental Bulletin* **17**, 2109–2121.

Zheng, M. X., Lian, F. L., Xiong, Y., Liu, B., Zhu, Y. J., Miao, S., Zhang, L. T. & Zheng, B. D. 2019 The synthesis and characterization of a xanthan gum-acrylamide-trimethylolpropane triglycidyl ether hydrogel. *Food Chemistry* **272**, 574–579.

Zhou, D. 2014 Adsorption of crystal violet onto amino silica: optimization, equilibrium, and kinetic studies. *Desalination and Water Treatment* **52** (31), 6113–6121.

First received 12 May 2018; accepted in revised form 16 January 2019. Available online 24 January 2019